

# Ocean heat content variability in an ensemble of twentieth century ocean reanalyses

Eric de Boissésón<sup>1</sup>  · Magdalena Alonso Balmaseda<sup>1</sup> · Michael Mayer<sup>2</sup>

Received: 10 January 2017 / Accepted: 26 July 2017 / Published online: 4 August 2017  
© Springer-Verlag GmbH Germany 2017

**Abstract** This paper presents a ten-member ensemble of twentieth century Ocean ReAnalyses called ORA-20C. ORA-20C assimilates temperature and salinity profiles and is forced by the ECMWF twentieth century atmospheric reanalysis (ERA-20C) over the 1900–2010 period. This study attempts to identify robust signals of ocean heat content change in ORA-20C and detect contamination by model errors, initial condition uncertainty, surface fluxes and observing system changes. It is shown that ORA-20C trends and variability in the first part of the century result from the surface fluxes and model drift towards a warmer mean state and weak meridional overturning circulation. The impact of the observing system in correcting the mean state causes the deceleration of the warming trend and alters the long-term climate signal. The ensemble spread reflects the long-lasting memory of the initial conditions and the convergence of the system to a solution compatible with surface fluxes, the ocean model and observational constraints. Observations constrain the ocean heat uptake trend in the last decades of the twentieth century, which is similar to trend estimations from the post-satellite era. An ocean heat budget analysis attributes ORA-20C heat content changes to surface fluxes in the first part of the century. The heat flux variability reflects spurious signals stemming from ERA-20C surface fields, which in return result from changes in the atmospheric observing system. The influence of the temperature assimilation increments on the heat

budget is growing with time. Increments control the most recent ocean heat uptake signals, highlighting imbalances in forced reanalysis systems in the ocean as well as in the atmosphere.

**Keywords** Ocean reanalysis · Twentieth century record · Climate signals · Observing system changes

## 1 Introduction

Climate monitoring has been a growing activity over the last decades especially since the threat of climate change has been acknowledged by the general public (Trenberth et al. 2016). Reconstructing the past climate is essential as it helps understand whether the recently observed climate changes are the result of the long-term natural variability or whether their origin is anthropogenic. Climate reanalysis has been shown to be a great tool for climate reconstruction by optimally combining observations and climate models (Dee et al. 2014). The National Centers for Environmental Prediction (NCEP) and the European Centre for Medium-range Weather Forecasts (ECMWF) conducted extended climate reanalyses of the atmosphere over the twentieth century—using 20CR (Compo et al. 2011) and ERA-20C (Poli et al. 2016), respectively—using, as much as possible, a consistent set of conventional surface observations. Such reanalysis datasets showed ability to detect climate signals from intra-seasonal to decadal timescales and long term climate trends.

The ocean modelling community has been using surface forcing from atmospheric reanalyses to produce multi-decadal ocean model simulations and ocean reanalyses. Ocean model intercomparisons have been carried out in the context of the Coupled Model Intercomparison Project

---

✉ Eric de Boissésón  
Eric.Boisseson@ecmwf.int

<sup>1</sup> European Centre for Medium-Range Weather Forecasts, Reading, UK

<sup>2</sup> Department of Meteorology and Geophysics, University of Vienna, Vienna, Austria

Phase 6 (CMIP6) to investigate the origins and impacts of systematic model biases (Griffies et al. 2009, 2014, 2016; Danabasoglu et al. 2014). Intercomparisons of ocean reanalyses (Balmaseda et al. 2014; Palmer et al. 2014) have been coordinated by the CLIVAR Ocean Model Development Panel (<http://www.clivar.org/clivar-panels/omdp>) to help quantify uncertainty due to changes in the observing system, model bias, atmospheric fluxes and assimilation methods and to provide a measure of the quality of the reanalyses. Extended atmospheric reanalyses such as the above mentioned 20CR and ERA-20C are now providing surface forcing for century-long ocean model simulations and data assimilation experiments. Müller et al. (2015) conducted ocean simulations forced by 20CR and were able to link changes in water mass properties in the North Atlantic in the 1920s to sea level pressure variability. He et al. (2016) studied the impact of the atmospheric forcing on the intensity of the Atlantic Meridional Overturning Circulation (AMOC) in ocean hindcasts. Ocean data assimilation experiments were also conducted over the twentieth century. Giese et al. (2016) chose to only assimilate SST observations to produce an ensemble of ocean reanalyses over the last 200 years forced by the 20CR version 2. They successfully reconstructed the climate evolution of the upper-ocean temperatures and heat content. Yang et al. (2016) compared data assimilation strategies for historical ocean reanalyses using both SST and subsurface observations. Their results showed that model biases develop during the first half of the twentieth century. By the 1950s, as the ocean observing system starts covering large scale regions, the ocean reanalyses exhibit large variability. Such variability can be a consequence of the large increments produced by the data assimilation when confronted with an increasing number ocean observations. In this context, a better understanding of the relationship between ocean model dynamics and its response to the atmospheric forcing and the changes in the ocean observing system is crucial when aiming for an improvement of the next generation of ocean historical reanalyses.

This study investigates these aspects in the first 10-member ensemble of twentieth century ocean reanalyses produced at ECMWF as part of the EU-funded ERA-CLIM2 project, called Ocean ReAnalysis of the twentieth century (ORA-20C). Surface boundary conditions come from the ERA-20C atmospheric reanalysis. ORA-20C covers the period 1900–2010 and has been used to initialize the coupled ECMWF reanalysis system (Laloyaux et al. 2016) for extended climate reconstruction. The analysis provided here will serve as a reference to understand the behaviour of future coupled datasets (Laloyaux et al. 2017). This study attempts to identify the sources of uncertainty behind the climate signals detected in ORA-20C. The ensemble information in ORA-20C is used to highlight the

interaction between the model timescales and the evolving ocean observing system. An ocean heat budget study is carried out to assess to what extent interannual-to-decadal signals detected in the reanalysis fields are affected by the model drift, the ocean observing system and the atmospheric forcing, respectively. Such a study also provides the first assessment of the ERA-20C atmospheric reanalysis surface fields from the perspective of the response of the ocean subsurface.

In the following, Sect. 2 describes the configuration and initialization strategy used to produce ORA-20C. Section 3 focuses on the ocean heat content (OHC) from ORA-20C. Sensitivity to model drift, climate variability and long-term trends are addressed and comparisons with respect to external products are carried out. Section 4 presents an ocean heat budget study for the attribution of interannual-to-decadal signals in the OHC. Section 5 summarizes and draws the conclusions from this work.

## 2 ORA-20C production

### 2.1 Configuration

ORA-20C reanalysis is conducted using the NEMO framework version 3.4 (Madec 2008). The ORCA1Z42 configuration used here corresponds to a  $1^\circ$  horizontal resolution with a refined mesh in the Tropics and 42 vertical levels with a first layer of 10-m thickness. NEMO includes the Louvain-la-Neuve Sea Ice Model (LIM) version 2 and active wave-ocean interactions using wave parameters from the atmospheric forcing (Breivik et al. 2015). ORA-20C upper boundary conditions come from 3-h surface fields from ERA-20C. Surface heat and freshwater fluxes are estimated with the CORE bulk formula (Large and Yeager 2004). The Sea Surface Temperature (SST) is constrained towards the control member of the HadISST2 monthly analysis (Titchner and Rayner 2014) by applying a surface heat flux correction (in  $\text{Wm}^{-2}$ ). This correction is estimated as the difference between the model SST and the HadISST2 analysis multiplied by a relaxation coefficient (here equal to  $-200 \text{ Wm}^{-2} \text{ K}^{-1}$ , corresponding to a 2–3 day relaxation timescale). The Sea Surface Salinity (SSS) is constrained towards the SSS climatology from the World Ocean Atlas 2013 (Locarnini et al. 2013) (WOA13) by applying a fresh water flux correction (in  $\text{mm day}^{-1}$ ). This correction is estimated as the difference between the model SSS and the SSS climatology from WOA13 multiplied by a relaxation coefficient (here  $-33 \text{ mm day}^{-1}$ , corresponding approximately to a 1-year timescale). A weak 3D relaxation to subsurface temperature and salinity climatologies from the WOA13 is also applied. The restoration factor is in  $\text{s}^{-1}$  and its strength is proportional the inverse of the relaxation timescale

(20 years in that case). It means that with idealized climatological forcing the model would converge to the specified climatological values in about 20 years. This term was introduced as a way to stabilize the system in long runs, but allowing decadal variability. The ORA-20C ensemble uses perturbations on the SST and surface fluxes generated following the method used by Hirahara et al. (2016).

### 2.2 Data assimilation and observations

ORA-20C assimilates ocean subsurface conventional observations with the NEMOVAR data assimilation system using a 3D-VAR with a First Guess at Appropriate Time (FGAT) approach (Weaver et al. 2003, 2005; Vialard et al. 2003; Ricci et al. 2005; Daget et al. 2009). The use of NEMOVAR at ECMWF is thoroughly described in Mogensen et al. (2012), Balmaseda et al. (2013a) and Zuo et al. (2015), and hence only a broad description of the data assimilation procedure is provided here. A first free-model trajectory (first guess) is used to estimate the model departures with respect to the observations. The data assimilation algorithms minimize a cost function ensuring optimal use of both observations and model physics. This procedure provides an increment that is applied to the vector of state variables of the ocean model (temperature, salinity, ocean currents and sea level) to produce the ocean analysis.

The increment fields from NEMOVAR are archived and monthly averaged. The temperature assimilation increment fields (in  $K day^{-1}$ ) and their impact on the OHC and the ocean heat budget are discussed in Sects. 3 and 4.

In ORA-20C, NEMOVAR assimilates ocean temperature and salinity profiles with a 1-month data assimilation window. Observations come from the UK MetOffice EN4.0.2 dataset (Good et al. 2013) that uses a bias correction for bathythermograph data from Gouretski and Reseghetti (2010). The number of profiles is very low in the first part of the twentieth century (Fig. 1a) with most observations close to the coast in the Northern Hemisphere. The observing system grows with time (Fig. 1b, c) with more and more measurements from eXpandable BathyThermograph (XBT) and conductivity temperature and depth (CTD) devices. The Southern Ocean remains poorly observed until the late 1990s. By the end of the ORA-20C period, the tropical arrays of mooring buoys and the Argo profiling floats provide a relatively good coverage of the global ocean (Fig. 1d).

### 2.3 Initialization

Initialising ORA-20C is a challenge because of the poor knowledge of the ocean state and the weak observational constraint in the early twentieth century. The ORA-20C

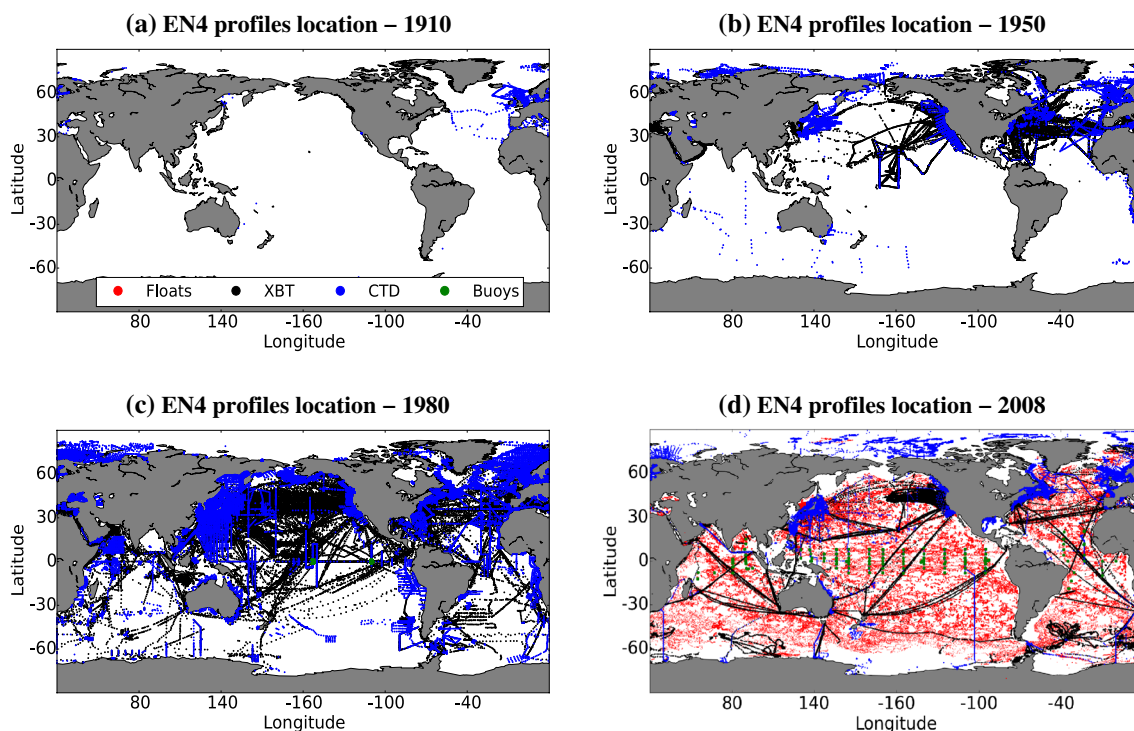


**Fig. 1** Profile locations in the EN4 dataset for the years **a** 1910, **b** 1950, **c** 1980 and **d** 2008. Profiles from CTD are in blue, XBT in black, buoys in green and floats in red

ensemble should take into account such uncertainty and start from initial conditions covering a wide range of plausible ocean properties and dynamics for January 1900. Such initial conditions are produced following a two-step process summarized in Fig. 2. A first twentieth century ocean model experiment without assimilation (referred to as NoDA in the next sections) is conducted over the 1900–2010 period starting from initial conditions from ORAS4 (Balmaseda et al. 2013a) taken on 1st January 1979. The mismatch of atmospheric conditions between 1900 and 1979 results in a spin-up of the model over the first decades of the twentieth century.

Assuming that the memory of the initial state has vanished in NoDA after the 1940s, the ocean state from 1st January 1959 is used to initialize three twentieth century Ocean Data Assimilation (ODA) experiments starting in 1900. These three ODA experiments use the same EN4 data and the same relaxation scheme as described in Sects. 2.1 and 2.2. The first experiment is a control ODA run (NoBC). In the second (BC1) and the third (BC2) ODA experiments, the bias correction scheme developed by Balmaseda et al. (2007) is activated. This scheme aims to

correct for temperature and salinity biases in the extra-tropical regions and applies a pressure correction in the tropical regions. The bias term is the sum of an offline bias estimated as the monthly climatology of the ocean assimilation increments from a pre-production run over a well-observed recent period (here 1989–2008) and an online bias which is updated each analysis cycle. More details on the use of bias correction in NEMOVAR can be found in Mogensen et al. (2012) and Zuo et al. (2015).

Two different climatological biases are estimated from pre-production experiments forced by ERA-Interim (Dee et al. 2011) and ERA-20C, respectively, and applied in the BC1 and BC2 runs. NoBC, BC1 and BC2 show sensitivity to the bias correction settings in the poorly-observed early twentieth century [see more details in de Boissésou and Balmaseda (2016)], displaying a wide range of ocean states in terms of OHC (Fig. 3a) and Atlantic Meridional Overturning Circulation (AMOC, Fig. 3b). Ocean states at dates sampling different OHC mean states and different phases of the AMOC are chosen as initial conditions for the 10 members of ORA-20C (see stars on Fig. 3). Ocean states from the 1st January 1936, 1st January 1940, 1st

**Fig. 2** Initialization procedure. A first twentieth century run without data assimilation (NoDA) is conducted. NoDA provides initial conditions for three twentieth century ODA runs. NoBC is a control ODA experiment. BC1 and BC2 use bias correction with different climatological components. NoBC, BC1 and BC2 provide the initial conditions for the ORA-20C ensemble members

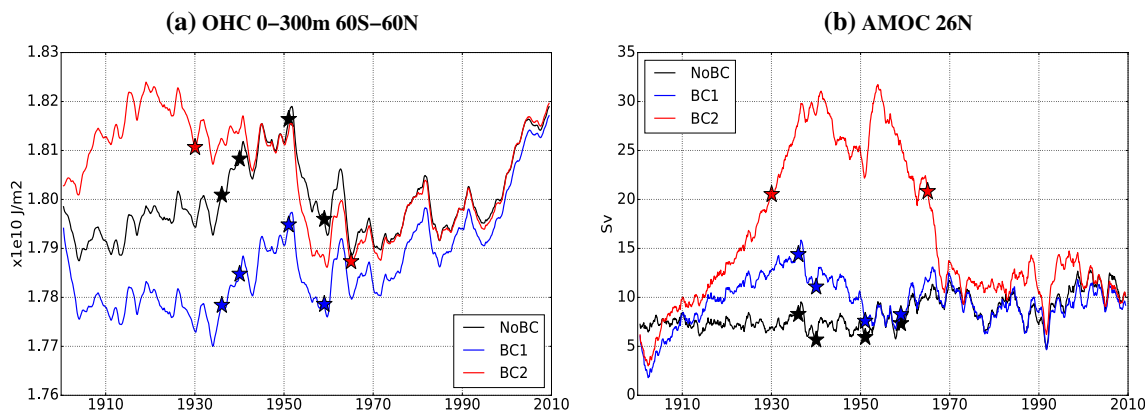
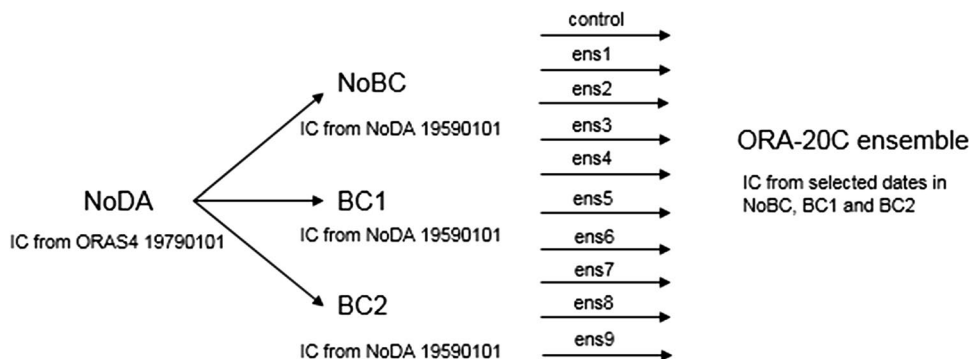


**Fig. 3** a Ocean heat content (in  $\text{Jm}^{-2}$ ) averaged between 60S–60N in the layer 0–300 m. Experiment NoBC (control ODA without bias correction) is in black. Experiment BC1 and BC2 (with bias correc-

tion) are in blue and red, respectively. Stars are located at the dates selected as initial conditions for the members of ORA-20C

January 1951 and 1st January 1959 are selected in experiments NoBC and BC1. As experiment BC2 showed strong sensitivity to the bias correction, we selected only two ocean states from the 1st January 1930 and 1st January 1965 that sample phases of large increase/decrease in the strength of the AMOC (Fig. 3b). The spread in initial conditions is assumed to be representative of the uncertainty in 1900. The bias correction is not used in ORA-20C for consistency purposes—the climatological bias of the well-observed period is not necessarily representative of the bias in the early twentieth century.

### 3 Ocean heat content in ORA-20C

The evolution of OHC has been tagged in several studies as an indicator of the ocean heat uptake (Willis et al. 2004; Gregory et al. 2004; Levitus et al. 2012; Balmaseda et al. 2013b; Durack et al. 2014; Cheng et al. 2015, 2017), a process that is instrumental in climate studies (Abraham et al. 2013; Palmer et al. 2015). In ORA-20C, the OHC gives an integrated view of long term signals and of the evolution of the ensemble spread.

### 3.1 Comparisons to other products

The OHC from ORA-20C is first compared to other products in the upper-ocean (0–300 m) to ensure its relevance. ORAS4 was the operational ECMWF ocean reanalysis until November 2016 (Balmaseda et al. 2013a). It has five members and was produced at the same resolution as ORA-20C from 1958 to present. Along with the EN4 temperature and salinity profiles, the Hadley Centre provides a monthly objective analysis (Good et al. 2013), referred to as EN4OA, that allows one to estimate area averaged heat content. It is worth noting that EN4OA relaxes to climatology in the absence of observations. The Simple Ocean Data Assimilation reanalysis version 2.2.4 (referred to as SODA, Carton and Giese 2008) is an ODA experiment conducted over the period 1871–2010 using 20CR atmospheric forcings and assimilating temperature and salinity from the World Ocean Database 2009 (Boyer et al. 2006). The upper-ocean heat content evolution in the different products is plotted as anomalies with respect to EN4OA average over 1970–2000 (Fig. 4a). In the first half of the twentieth century, the spread in OHC in ORA-20C is rather large with ORA-20C ensemble members

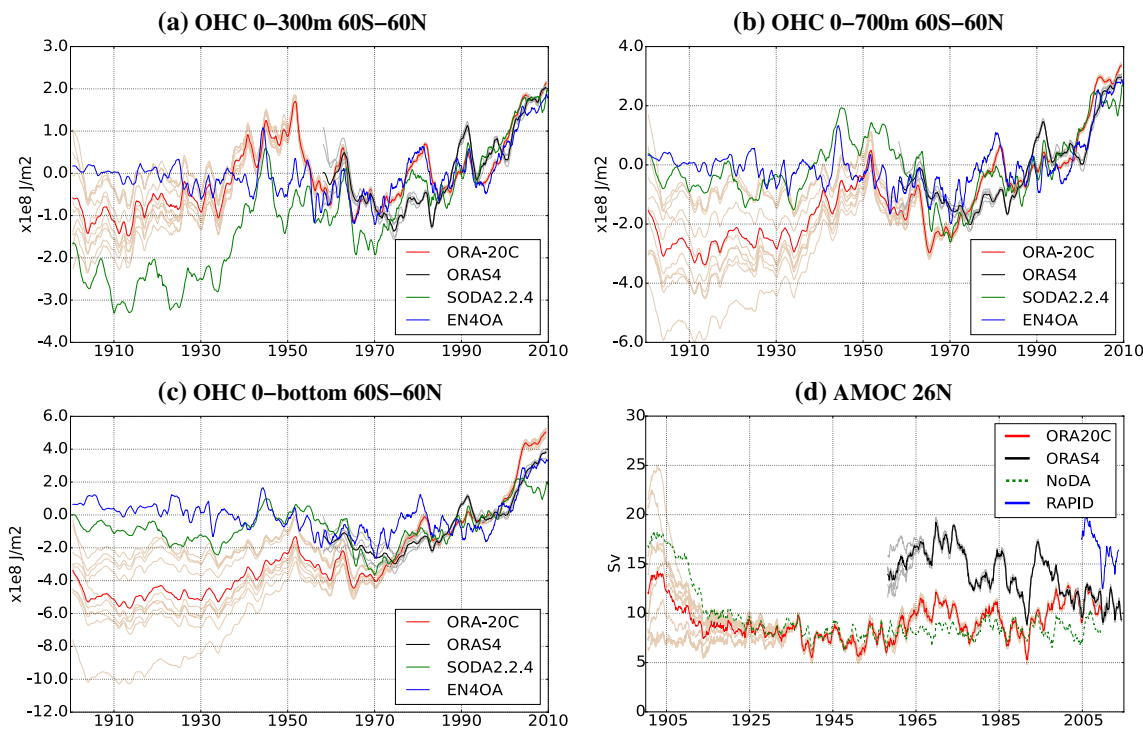


**Fig. 4** a–c Ocean heat content (in  $\text{Jm}^{-2}$ ) averaged between 60S–60N in a the layer 0–300 m, b the layer 0–700 m and c the total column. ORA-20C ensembles are in light red, ORA-20C ensemble mean in red, ORAS4 ensembles in grey, ORAS4 ensemble mean in black, SODA2.2.4 in green and EN4OA in blue. The heat content is plotted as an anomaly with respect to EN4OA average over 1970–2000 for

all the products. d Intensity of the northward transport (in Sv) of the upper branch of the AMOC across 26 N at 1000 m depth. ORA-20C ensembles are in light red, ORA-20C ensemble mean in red, ORAS4 ensembles in grey, ORAS4 ensemble mean in black, the ocean experiment without ODA (NoDA) in dashed green and the measurements from the RAPID array in blue

lying somewhere in between EN4OA (which is pretty flat due to the relatively low number of available observations) and SODA. Both ORA-20C and SODA show a warming in the first half of the twentieth century that stopped between the 1950–1970s in agreement to what is seen at the surface in HadISST2 [Fig. 1 from Hersbach et al. (2015)]. This warming is not seen in EN4OA that mostly relaxes to climatology in that period. The upper-ocean warming in ORA-20C and SODA suggests a dynamical response of the model to the surface forcing and confirms the value of model-based ocean reanalyses with respect to observation-only products. In the last decades of the twentieth century, the upper-ocean heat content shows a similar warming trend in all products suggesting a very robust signal. When considering deeper layers (Fig. 4b, c), differences between products get larger in the poorly-observed early twentieth century. In the latter period, all products are consistent in showing a warming trend. It is worth noting that, when considering the whole water column, ORA-20C shows a substantially

stronger heat uptake in the 2000s than what is seen in SODA, ORAS4 and EN4OA.

### 3.2 Impact of the data assimilation on the representation of accelerated warming periods

The upper ocean (0–300 m) in ORA-20C shows a warming trend in the early twentieth century that is stopped in the mid-1950s (Fig. 5a). The OHC then drops to values as low as those seen in the 1930s before increasing again from the mid-1970s onwards. Similar OHC levels as in the 1950s are only reached in the 2000s after a period of accelerated warming starting in the late 1990s. The coincidence between the drop in OHC and the start of the relatively well-observed period suggests a shock due to data assimilation. The first twentieth century ocean experiment without ODA conducted within the initialisation procedure (referred to as NoDA in Sect. 2.3) can help testing this hypothesis. The global OHC in NoDA behaves similarly

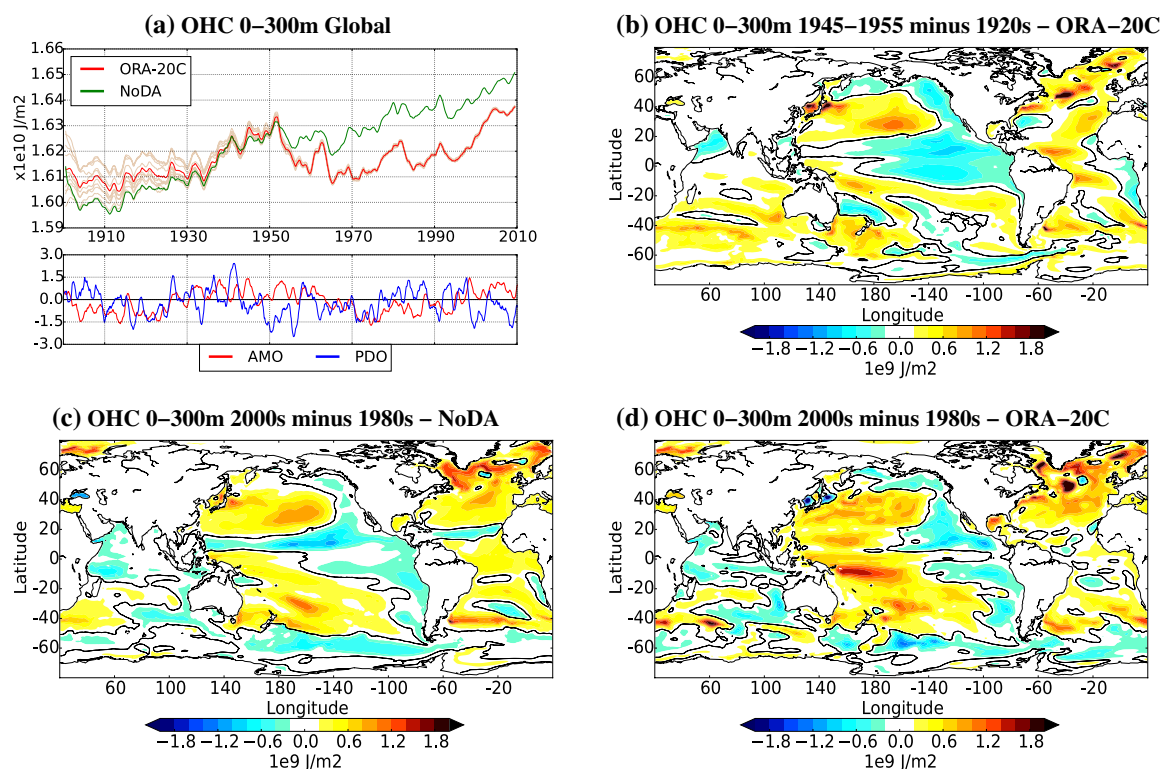


**Fig. 5** **a** Upper panel global (90°S/90°N) average of the ocean heat content (in  $\text{Jm}^{-2}$ ) for the layer 0–300 m in ORA-20C (ensemble mean in red and individual ensembles in light red) and in the ocean experiment without ODA (NoDA, green); lower panel monthly indices of Pacific Decadal Oscillation (PDO, blue) and Atlantic Multidecadal Oscillation (AMO, red). These indices were retrieved from the National Oceanic and Atmospheric Administration (NOAA) website. The PDO index is estimated as the leading principal component of North Pacific monthly sea surface temperature variability (poleward

of 20°N for the 1900–1993 period). The AMO index is estimated as a smoothed and detrended area weighted average of the SST over the North Atlantic (0–70°N). **b** Difference (in  $\text{Jm}^{-2}$ ) between the ocean heat content averaged over the period 1945–1955 and its average over 1920s in ORA-20C control member for the layer 0–300 m. **c**, **d** Difference (in  $\text{Jm}^{-2}$ ) between the ocean heat content averaged over the 2000s and its average over the 1980s in ORA-20C control member and NoDA, respectively, for the layer 0–300 m

to ORA-20C over the period 1910–1950 (Fig. 5a), showing a slow upper-ocean warming until the late 1920s and an accelerated warming from the mid-1920s to the mid-1950s. The spatial pattern of this accelerated warming is represented on Fig. 5b (only ORA-20C shown) as the difference in upper-ocean heat content between the 1920s and the 1945–1955 period. This difference shows a “horseshoe” pattern of cooling temperature in the North Pacific that is reminiscent of a transition from a positive to a negative phase of the Pacific Decadal Oscillation (PDO, Mantua and Hare (2002), see index on Fig. 5a lower panel). Over the 1950–1970 period, the upper-ocean heat content from NoDA remains relatively stable (Fig. 5a). This suggests that the cooling seen in ORA-20C over that period is a response to the assimilation of a relatively large number of ocean observation that corrects the mean state of the model. The OHC in NoDA then grows steadily from the mid-1970s onwards. Unlike ORA-20C, the accelerated period of warming from the late 1990s onwards just continues the longer term signal. The spatial pattern of this recent warming again bears some marks of the transition to form a positive (prior to the late 1990s) to a negative PDO phase (from the late 1990s onwards) in both NoDA and ORA-20C (Fig. 5a, c, d). The general warming in the North Atlantic is also consistent with the transition from a negative (from the

1980s to the mid-1990s) to a positive phase (from the mid-1990s onwards) of the Atlantic Multidecadal Oscillation [AMO on Fig. 5a, Enfield et al. (2001)].

### 3.3 Evolution of the ocean heat content spread

In the first part of the twentieth century, the OHC spread in the ORA-20C ensemble is larger than the amplitude of the interannual-to-decadadal variability (Fig. 4a–c). In the second half of the period, the spread rapidly reduces and ensemble members are all very close to the ensemble mean. The time evolution of the spread depends on the state of the observing system but also on the model inertia. In the early twentieth century, the poor observing system cannot constrain the wide range of ocean initial states and the model needs time to adjust. The spatial pattern of the spread in the upper 700 m (Fig. 6a) shows relatively large values in the subpolar North Atlantic and the Tropical Atlantic (in particular in the Brazil-Malvinas confluence and along the Benguela Current). Those are key areas for the AMOC that also shows large spread in intensity at 26 N (Fig. 4d) from 1900 to 1915. Most of the spread comes from the choice of the initial conditions and disappears in the 1930s as ORA-20C members converge. This rapid convergence suggests that the model,

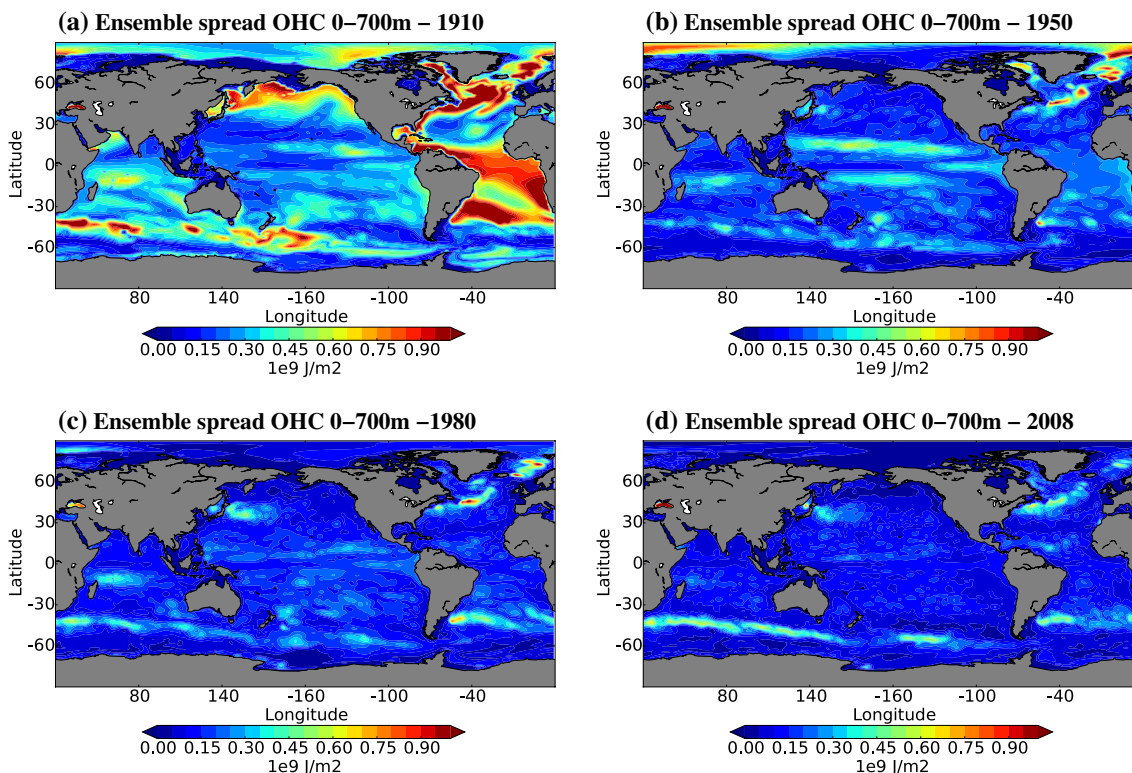


**Fig. 6** Ensemble spread of the heat content of the layer 0–700 m (in  $J/m^2$ ) in ORA-20C for the years **a** 1910, **b** 1950, **c** 1980 and **d** 2008. The spread is estimated as the standard deviation among annual averages of ORA-20C members

unconstrained by observations, is drifting towards its preferred state with weak meridional circulation (as seen in NoDA, Fig. 4d). Large spread is also found in the subpolar North Pacific and the Southern Ocean along the path of the Antarctic Circumpolar Current (ACC, Fig. 6a). With time, the number of observations is getting larger and the memory of the initial state is vanishing. By the 1950s, the ensemble spread is largely reduced, especially in the subtropics (Fig. 6b). The tropical basins still show some spread, suggesting that adjustments are still ongoing there and that the observational constraint is not strong enough to constrain the wind forced circulation. In the 1980s (Fig. 6c), the tropical spread has lowered. The remaining spread is now found in the Western Boundary Currents, along the North Atlantic Current, in the Nordic Seas and along the ACC. In the 2000s, the strong increase of available Argo data substantially reduces the ensemble spread on a global scale (Fig. 6d). Some spread is still found in the Southern Ocean where the sampling remains relatively poor (Fig. 1d), the ocean intrinsic variability is high (Penduff et al. 2011) and the position of the ACC has been changing over time (Gille 2002).

### 3.4 Long-term variability

Long term variability in ORA-20C gives insights into the behaviour of the system when transitioning from a poor to a relatively strong observational constraint. Figure 7 shows differences in OHC between the periods 1910–1940 and 1980–2010 for the ORA-20C control member. The upper ocean (0–300 m) overall shows a cooling in the tropics and a warming in the subtropics, particularly in the southern hemisphere (Fig. 7a). This hemispherical pattern is also a prominent feature in numerous free-ocean model (Durack et al. 2014). The ocean interior is warming in the tropical Indo-Pacific basin, suggesting some mixing between the surface and the subsurface (Fig. 7b). The tropical Atlantic is cooling from top to bottom. This behaviour is consistent with the transition from low to relatively high AMOC activity (Fig. 4d). Stronger AMOC involves a transfer of tropical waters towards the north Atlantic, while the return branch of the AMOC transports cold waters southward into the ocean interior.

The equatorial temperature section from Fig. 7c highlights a cooling along the thermocline suggesting more

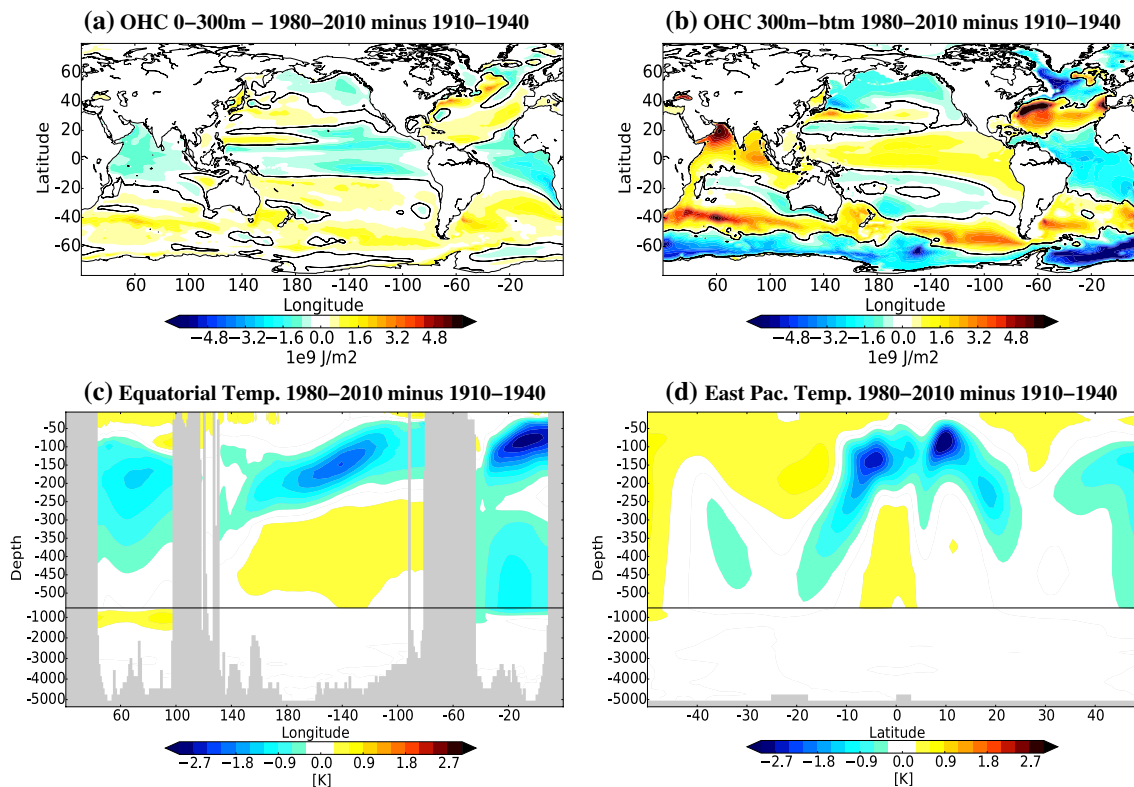


**Fig. 7** Difference (in  $\text{Jm}^{-2}$ ) between the ocean heat content averaged over the period 1980–2010 and its average over the period 1910–1940 in (a) the 0–300 m layer and (b) the 300 m–bottom layer. c Equatorial section (taken at 0°N) of the difference (in °C) between the temperature averaged over the period 1980–2010 and its average over

1910–1940 in ORA-20C control member. d Meridional section of the difference (in °C) between the temperature averaged over the period 1980–2010 and its average over the period 1910–1940 in ORA-20C control member. The difference in temperature is longitudinally averaged over the eastern Pacific (160°W–90°W)

stratification and stronger equatorial counter currents in the later decades of ORA-20C. The eastern Pacific meridional section (Fig. 7d) shows that the cooling pattern is following the shape of the thermocline slope towards the subtropics and is topped by a warming signal. This pattern suggests a strengthening of the subtropical gyre circulation in the Pacific. Part of the equatorial cooling is related to the temperature assimilation increments, in particular in the Pacific basin (Fig. 8). When the observational constraint is low (like in the 1910–1940 period), the ocean model cannot capture the correct equatorial thermocline (Fig. 8c). The assimilation of a relatively large number of observations in the second half of the twentieth century produces strong assimilation increments that bring the model closer to the observed state. This kind of model bias could be reduced with a suitable bias correction scheme as shown in Balmaseda et al. (2007).

Cold assimilation increments are very much localised at the Equator (Fig. 8). In the subtropics, assimilation increments are mostly positive (yellow to red colours on Fig. 8a)

compensating for a trend toward negative surface heat flux (the ocean loses heat, blue colours on Fig. 9a). This heat loss is consistent with a strengthening of the large-scale surface atmospheric circulation in ERA-20C as shown by the zonal wind stress trend (Fig. 9b). Stronger westerlies in the subtropics and easterlies in the tropics can explain the increased gyre circulation. Equatorial counter currents also intensify as a response to warm surface waters being pushed to the western side of the basins. In the tropical Pacific, opposite trends in zonal wind stress in the western and eastern part of the basin indicate a trend toward wind divergence reminiscent of a La Niña-Modoki situation (Ashok and Yamagata 2009) that would favour upwelling in the Nino 3.4 region.

As a response to the increased wind forcing, the subtropical Pacific and Atlantic Basins show cooling over almost the whole water column (Fig. 7a, b). Stronger westerly wind stress, negative temperature assimilation increments and heat loss over the Atlantic subtropical gyre (Figs. 8a, b, 9a, b) favour deep convection and the strengthening of

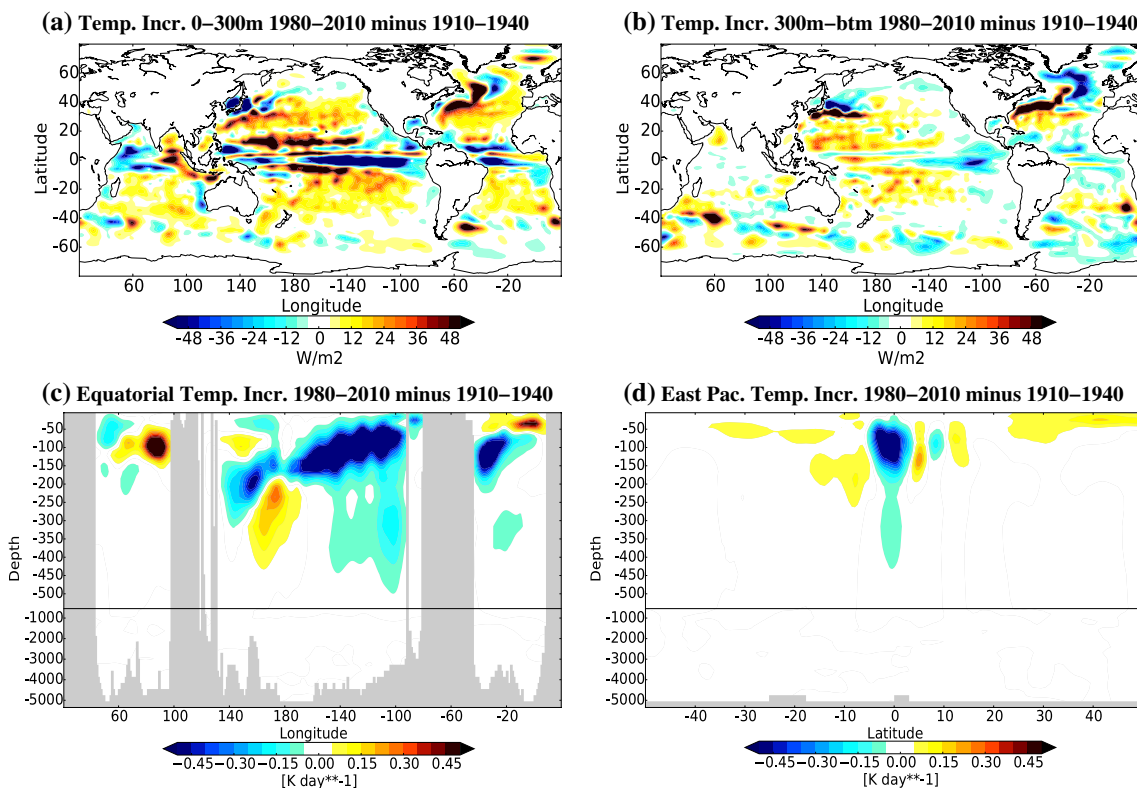


**Fig. 8** Difference (in  $Wm^{-2}$ ) between the temperature assimilation increments averaged over the period 1980–2010 and their average over the period 1910–1940 in ORA-20C control member for **a** the 0–300 m layer and **b** the 300 m-bottom layer. The temperature assimilation increments are transformed from  $K day^{-1}$  to  $Wm^{-2}$  by integrating them over the corresponding layer and multiplying them by the sea-water density and heat capacity. **c** Equatorial section (taken at 0 N) of the difference (in  $K day^{-1}$ ) between the temperature assi-

lation increments averaged over the period 1980–2010 and their average over the period 1910–1940 in ORA-20C control member. **d** Meridional section of the difference (in  $K day^{-1}$ ) between the temperature assimilation increments averaged over the period 1980–2010 and their average over the period 1910–1940 in ORA-20C control member. The difference in temperature increments is longitudinally averaged over the eastern Pacific (160W–90W)

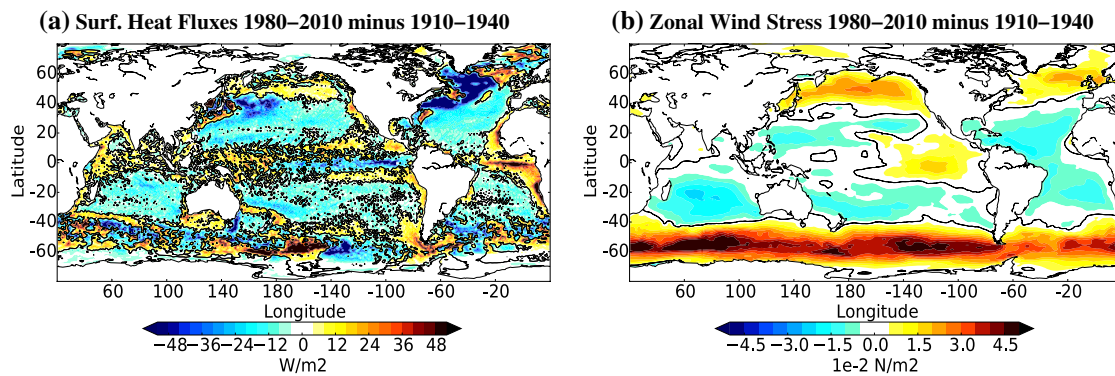


**Fig. 9** **a** Difference (in  $\text{Wm}^{-2}$ ) between the surface heat fluxes averaged over the period 1980–2010 and their average over the period 1910–1940 in ORA-20C control member. **b** Difference (in  $\text{Nm}^{-2}$ ) between the zonal wind stress averaged over the period 1980–2010

and its average over the period 1910–1940 in ORA-20C control member. Positive (negative) wind stress differences indicate stronger westerlies (easterlies)

the AMOC in the late decades of ORA-20C (Fig. 4d). The strong wind stress signal seen over the southern Ocean coincides with the strengthening of the polar vortex linked with the negative trend in sea level pressure seen in the ERA-20C forcing (Poli et al. 2015). This intensifying of westerlies may explain the cooling (warming) seen south (north) of the deep ACC (Fig. 7b) that suggests a strengthening of the polar front.

#### 4 Ocean heat budget diagnostics for the attribution of interannual-to-decadal ocean heat content signals in ORA-20C

As seen in Sect. 3.4, OHC variability in ORA-20C results from changes in the forcing and in the ocean temperature assimilation increments. Poli et al. (2015) show that the atmospheric temperature increment in ERA-20C has an impact on the surface heat fluxes as the lower boundary condition is fixed and cannot react to this increment. The surface variables from ERA-20C used to estimate the heat fluxes at the air-sea interface will transfer the influence of the atmospheric observations to the ocean heat budget. The ocean temperature assimilation increments and relaxation terms are responding both to the atmospheric forcing and changes in the ocean observing system. The ocean heat budget is then affected both by the ocean (directly) and atmospheric (indirectly) observing systems.

##### 4.1 Global heat budget

On a global scale, changes in OHC equal the sum of the heat fluxes at the air-sea interface (positive downward), the flux correction from the SST relaxation, and the integrated temperature assimilation increment and relaxation to climatology. The global ocean heat budget estimated offline from

ORA-20C outputs is closing pretty well (residuals lower than  $\pm 0.5 \text{ Wm}^{-2}$ , Fig. 10a). The two largest terms of the budgets are net heat flux term (radiative plus turbulent flux) that is on average negative around  $-10$  to  $-20 \text{ Wm}^{-2}$  and the flux correction associated to the SST relaxation term that is on average positive around  $10$ – $15 \text{ Wm}^{-2}$ . These two terms explain most of the total OHC changes up to the end of the Second World War. From then on, the impact of the temperature assimilation increment gains more and more importance (Fig. 10a). The surface heat flux term bears the marks of the lack of atmospheric observations during the two World Wars (Fig. 11c) with stronger heat transfer from the ocean to the atmosphere (Fig. 10a). These two events are compensated by the SST relaxation term that constrains the ocean surface towards the HadISST2 analysis. The total heat flux term (net heat flux plus SST relaxation) shows a continuing decreasing trend following the Second World War that is compensated by an increasing trend in the ocean temperature increment (Fig. 10a). The two World War signals and the decreasing trend in heat fluxes are dominated by the surface latent heat fluxes in response to variations in surface wind intensities in ERA-20C (Fig. 11a, b). The wind speed changes are likely to be linked to changes in the marine wind observations. The signals coinciding with the World War periods reflect a sudden decrease in the number of marine wind observations at that time (Fig. 11c). The intensification of the surface wind seen in the second part of the twentieth century (Fig. 11b) coincides with measurements from ships getting higher as the anemometer heights increase with time (Thomas et al. 2008).

##### 4.2 Regional heat budget

Regional heat budgets give additional insights into the impact of the observing systems on the ocean state. The residual of such budgets provides an indirect estimate

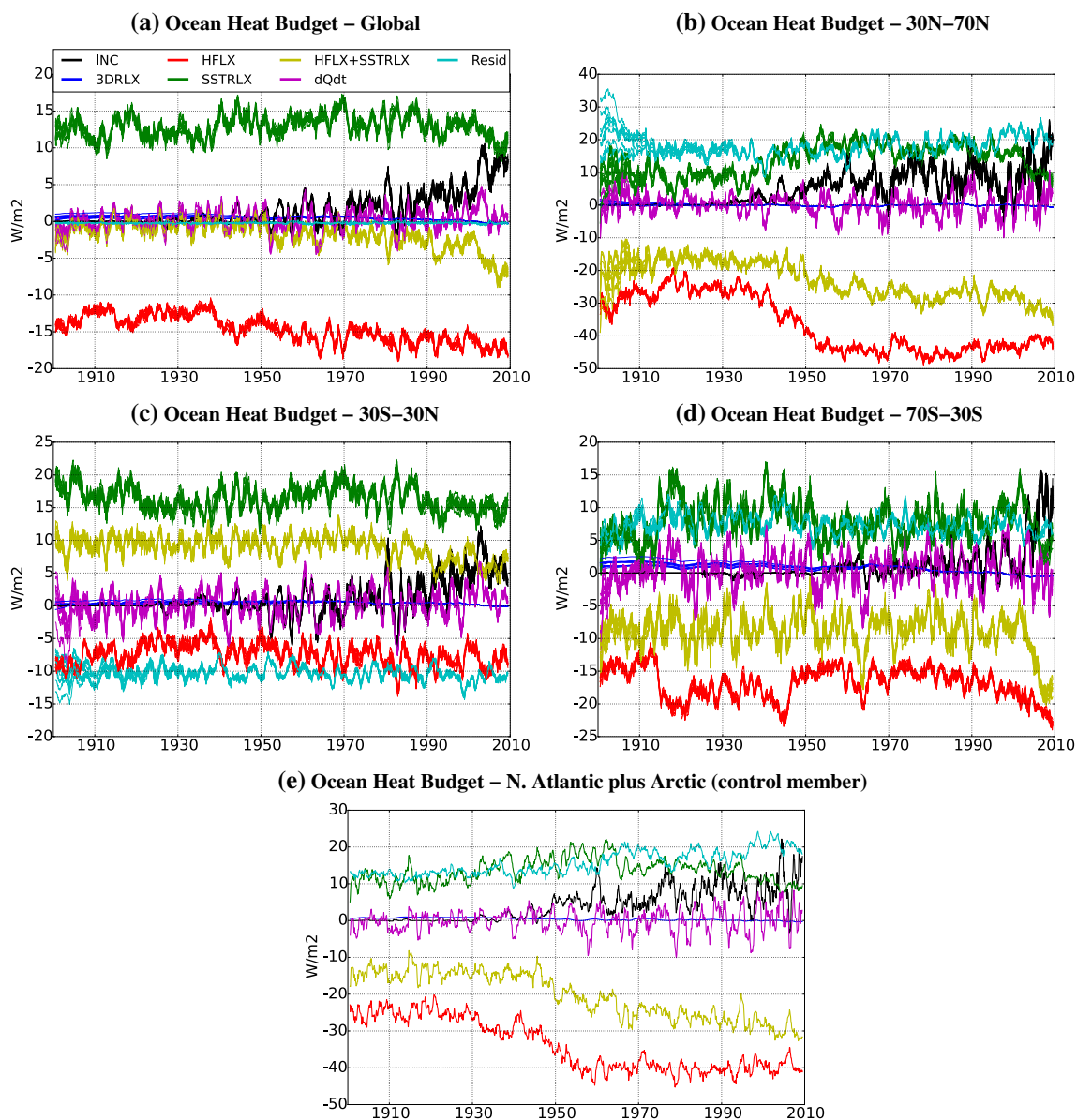


**Fig. 10** Total column ocean heat budget for ORA-20C ensemble members in the **a** global ocean, **b** the Northern extra-Tropics (30N–70N), **c** the Tropics (30S–30N) and **d** the Southern extra-Tropics (70S–30S). **e** Similar heat budget for the North Atlantic plus Arctic basins (bounded by 30N and the Bering Strait) for ORA-20C control member. The terms of the budget are in  $W/m^2$ . The depth integrated assimilation increment is in black. The depth integrated relaxation to the temperature-and-salinity climatology from WOA13 is in blue. The net ocean surface heat flux (positive downward) is in red. The

flux correction associated with the relaxation to the HadISST2 analysis is in green. The sum of the surface heat flux and its correction by the SST relaxation is in yellow. The temporal variations of ocean heat content are in magenta. The residual of the budget is in cyan. For regional heat budgets, the residual is an indirect estimate of the convergence of horizontal ocean heat transport within the region of interest. A positive residual indicates convergence of heat transport whereas a negative residual indicates divergence of heat transport in the region of interest

of the convergence of horizontal ocean heat transport within the region of interest (cyan curves on Fig. 10a–e). In the Northern extratropics (30N–70N), the impact of the increasing wind speed from ERA-20C (Fig. 11a, b) is clearly seen in the heat flux term (through the latent heat flux) that shows a sudden drop in the 1940s (Fig. 10b). This drop is compensated both by the SST relaxation and

the temperature assimilation increment. The contribution of the temperature assimilation increment starts being substantial (around  $10 Wm^{-2}$ ) as early as the 1950s thanks to the relatively good observational coverage at these latitudes (Fig. 1b). The convergence of the horizontal heat transport between 30 N and 70 N (Fig. 10b) shows a large spread at the start of the period, reminiscent of the AMOC spread

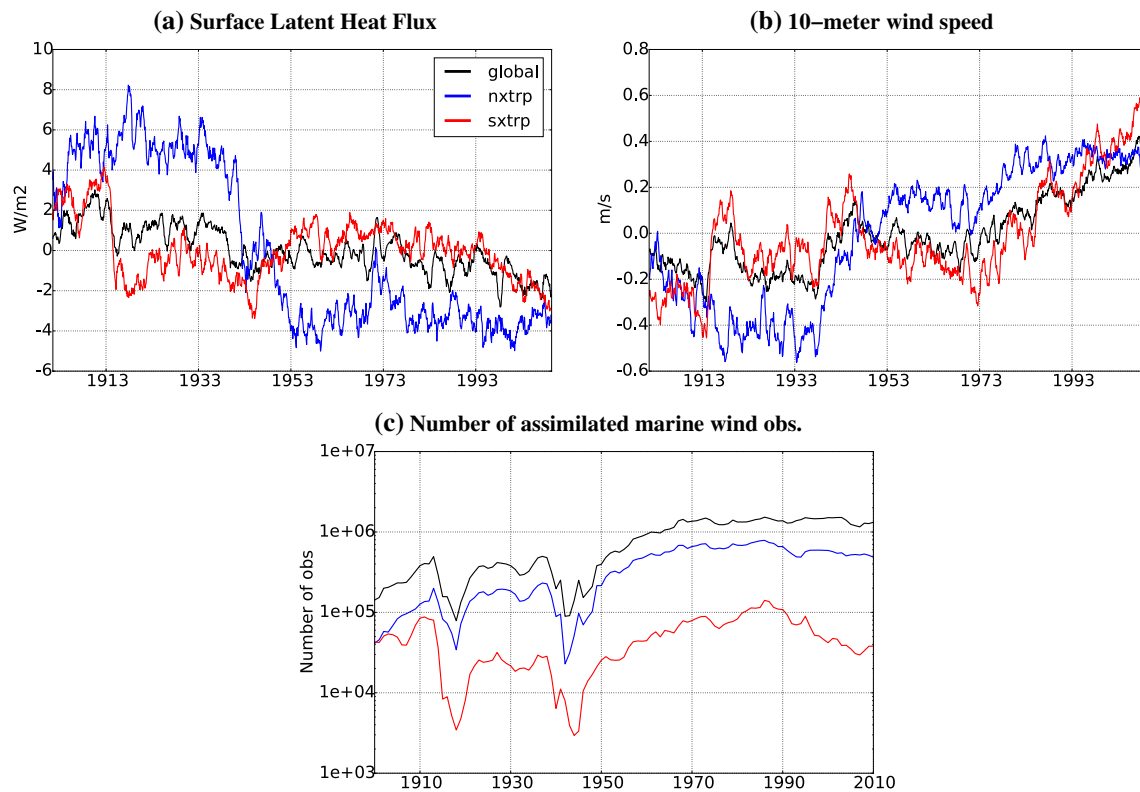


**Fig. 11** Anomalies with respect to the 1900–2010 mean of **a** the surface latent heat fluxes (in  $\text{Wm}^{-2}$ ) and **b** the 10-m wind speed (in  $\text{ms}^{-1}$ ) from ERA-20C deterministic. The anomalies are averaged over the global ocean (*black*), the Northern extratropics (30N–70N, *blue*)

and the southern extratropics (70S–30S, *red*). **c** Number of assimilated marine wind observations from International Comprehensive Ocean–Atmosphere Data Set (ICOADS) assimilated in ERA-20C for the same regions as in **a**, **b**

seen on Fig. 4d. The heat transport convergence contribution is positive around  $15 \text{ Wm}^{-2}$  in the early twentieth century. In the second half of the century the heat transport convergence has long periods over  $20 \text{ Wm}^{-2}$ , suggesting enhanced meridional exchanges between tropics and subtropics. We additionally diagnosed the heat budget of the North Atlantic plus Arctic basins (bounded by 30 N and the Bering Strait; for the control member only, Fig. 10e). The convergence of horizontal ocean heat transport (cyan curve on Fig. 10e) is a good indicator of the northward transport of heat across 30 N as the transport through the Bering Strait is comparatively small (not shown). The heat transport increase across 30 N from the 1950s is consistent with the strengthening of the upper branch of the AMOC advecting warm tropical waters poleward (Fig. 4d).

In the Tropics (30S–30N, Fig. 10c), the convergence of the horizontal heat transport is negative around  $-10 \text{ Wm}^{-2}$  as warm waters are advected poleward. The temperature assimilation increments start to really affect the heat budget from the 1990s onward with the deployment of the Tropical moored buoy arrays. In the Southern extratropics (70S–30S), the net heat flux term is strongly reacting to signals in the latent heat fluxes during the two World Wars

(Figs. 10d, 11a). These signals are mainly driven by abrupt changes in surface wind speed (Fig. 11b) that are linked with the drop in available marine wind observations during these periods (Fig. 11c). The SST relaxation term compensates for the changes in surface heat fluxes to keep the SST close to observations. The convergence of the horizontal ocean heat transport is positive around  $8 \text{ Wm}^{-2}$  with heat transferred from the Tropics towards higher latitudes. The temperature assimilation increment is on average relatively low due to the poor observation sampling (Fig. 1a–c). The deployment of Argo floats in the early 2000s (Fig. 1d) coincides with strong positive temperature assimilation increments and subsequent adjustments in net heat fluxes and SST relaxation (Fig. 10d).

## 5 Summary and discussion

This study presents the ensemble of twentieth century ocean reanalyses—called ORA-20C—conducted at EMCWF using ERA-20C (Poli et al. 2016) as surface boundary conditions. The primary purpose of such an exercise is to provide a twentieth century record of ocean

states for climate reconstruction and initialization of coupled ocean–atmosphere data assimilation experiments (Lalouaux et al. 2016, 2017). The evolution of the ensemble information shows a system that is mainly controlled by the surface fluxes in the first half of the century. It takes a few decades for the memory of the initial conditions to vanish as the model is drifting towards its own climate. In spite of model biases and drift, the pattern of upper-ocean warming detected in ORA-20C from 1910 to 1950 is consistent with climate indices such as the PDO and the AMO (Figs. 4, 5). As the ocean observing system grows, assimilation increments have more impact on the ocean state. The transition from weak to relatively strong observational constraint causes a cooling in ORA-20C and a deceleration of the subsequent warming trend from the 1970s to the mid-1990s. In the last decades of ORA-20C, the ocean heat uptake pattern is however consistent with the literature (Levitus et al. 2012; Balmaseda et al. 2013b; Rhein et al. 2013) and suggests links with PDO and AMO switching phases.

The transition from the poor to relatively strong observational constraints is a challenge in twentieth century ocean reanalyses. The unconstrained ocean model needs to be realistic enough to avoid spurious signals when observations become available (i.e. assimilation increments begin to alter the ocean mean state). In ORA-20C, the intensity of the AMOC can be up to 50% weaker in the sparse data period (and even more when compared to ORAS4 or the RAPID array, Fig. 4d) than in the well-observed period leading to spurious trends in water mass properties (Fig. 7a, b). Underestimated AMOC intensities are a common issue in ocean models at a 1-degree resolution (Danabasoglu et al. 2014). Higher model resolution (Stepanov and Haines 2014; Talandier et al. 2014) and a better treatment of sea-ice (Vancoppenolle et al. 2009) can help improving the representation of the North Atlantic Ocean dynamics and freshwater balance that are crucial aspects for a realistic AMOC (Huang et al. 2015). In the meantime, Yang et al. (2016) discuss the possible implementation of a bias correction scheme to reconstruct a better ocean state in poorly-observed periods. Adapting schemes such as those developed by Balmaseda et al. (2007) for ORAS4 would probably help reducing the tropical bias and correct for the position of the equatorial thermocline (Fig. 7c). Variational techniques inspired from atmospheric reanalyses (Dee et al. 2011) could also be options to investigate in future extended ocean reanalyses.

ORA-20C provides an assessment of the surface forcing from ERA-20C from the perspective of the ocean. The heat budget study carried out for ORA-20C shows that ERA-20C heat fluxes are affected by spurious signals and trends in the first half of the twentieth century that are damped by the SST relaxation (Fig. 10). These signals seem to be

linked to the evolving number and quality of wind speed observations assimilated in ERA-20C (Fig. 11). A lot of factors affect the quality of conventional surface wind observations (Ingleby 2010). Winds from buoys and drifters can be affected by the sea state while consistency in measurements from ships suffer from changes in measurement method (from visual to automated) and in the height of the vessels (Kent et al. 2007). While the wind assimilation improves the quality of the atmospheric circulation in ERA-20C (Poli et al. 2013), consistency issues in the observed wind record affect the surface heat fluxes and thus the ocean heat budget. Thomas et al. (2008) showed that consistency could be improved with adjustments methods for wind measurements from ships. Following different approaches, Berry and Kent (2010) and Tokinaga and Xie (2011) produced multi-decadal observation-based analyses of surface wind speed with bias corrections. Similar methods for bias correction could be used in climate reanalyses to improve the consistency of the air-sea fluxes.

As the number of ocean observations is increasing, the contribution of the temperature assimilation increments to the ocean heat budget is growing. From the 1950s onwards, the depth-integrated temperature assimilation increment shows a positive trend that compensates for a negative trend in surface fluxes (Fig. 10a). The heat content increase in the last decades of ORA-20C is mainly controlled by the assimilation increment instead of the downward surface heat fluxes, which indicates serious deficiencies in ocean models and surface fluxes. The compensation between surface fluxes and temperature assimilation increments is a common feature to a lot of ocean reanalysis products (Valdivieso et al. 2015), suggesting inconsistencies at the air-sea interface. Poli et al. (2016) showed that ERA-20C surface fluxes are influenced by the atmospheric assimilation increment as the surface boundary condition is fixed. In ORA-20C, the atmospheric surface variables are fixed and cannot respond to the ocean changes that will then affect the surface heat fluxes. The heat budget study conducted here strongly suggests that the lack of dynamical interactions between ocean and atmosphere is leading to counter-intuitive behaviours.

Extending ocean reanalyses back in time using twentieth century atmospheric reanalyses as surface boundary conditions is a challenging exercise. Extended ocean reanalyses are useful to test data assimilation strategies (Yang et al. 2016), monitor climate signals in the ocean (Giese et al. 2016), and assess the impact of the observing system changes on the reconstruction of the ocean over the past century. ORA-20C is the first ensemble of ocean reanalyses forced by the ERA-20C atmospheric reanalysis. It provides estimates of the ocean states over the 1900–2010 period. The analysis of climate signals and long-term trends highlights the challenges that remain to be tackled to make

substantial progress in the extended climate reanalysis fields. The ERA-20C atmospheric reanalysis is for the first time assessed from the perspective of the ocean highlighting the limitations of forced reanalyses products at the air-sea interface. These limitations argue for more coupling in the next reanalysis systems developed in numerical weather prediction centres. In that context, a twentieth century coupled ocean atmosphere reanalysis is being produced at ECMWF (Laloyaux et al. 2017). Comparisons with ERA-20C will help understand the potential benefits of a coupled approach.

**Acknowledgements** This work was EU-funded by the FP7 ERA-CLIM2 project. The contribution of M. Mayer was funded by the Austrian Wissenschaftsfonds (FWF project P28818-N29) and COST-EOS.

## References

- Abraham JP, Baringer M, Bindoff NL, Boyer T, Cheng LJ, Church JA, Conroy JL, Domingues CM, Fasullo JT, Gilson J, Goni G (2013) A review of global ocean temperature observations: implications for ocean heat content estimates and climate change. *Rev Geophys* 51(3):450–483
- Ashok K, Yamagata T (2009) Climate change: the El Niño with a difference. *Nature* 461(7263):481–484
- Balmaseda MA, Dee D, Vidard A, Anderson DLT (2007) A multivariate treatment of bias for sequential data assimilation: application to the tropical oceans. *QJR Meteorol Soc* 133:167–179. doi:10.1002/qj.12
- Balmaseda MA, Hernandez F, Storto A, Palmer M, Shi L, Smith G, Toyoda T, Valdivieso M, Alves O, Barnier B, Boyer T, Chang Y, Chepurin GA, Ferry N, Forget G, Fujii Y, Good S, Guinehut S, Haines K, Ishikawa Y, Keeley S, Köhl A, Lee T, Martin M, Masina S, Masuda S, Meyssignac B, Mogensen K, Parent L, Peterson KA, Yin Y, Vernieres G, Wang X, Waters J, Wedd R, Wang Q, Xue Y, Chevallier M, Lemieux J-F, Dupont F, Kuragano T, Kamachi M, Awaji T, Wilmer-Becker K, Gaillard F (2014) The Ocean Reanalyses Intercomparison Project (ORA-IP). *CLIVAR Exch* 19(1):3–7
- Balmaseda MA, Mogensen K, Weaver AT (2013a) Evaluation of the ECMWF ocean reanalysis system ORAS4. *QJR Meteorol Soc* 139:1132–1161. doi:10.1002/qj.2063
- Balmaseda MA, Trenberth KE, Källén E (2013b) Distinctive climate signals in reanalysis of global ocean heat content. *Geophys Res Lett* 40:1754–1759. doi:10.1002/grl.50382
- Berry DI, Kent EC (2010) Air–sea fluxes from ICOADS: the construction of a new gridded dataset with uncertainty estimates. *Int J Climatol*. doi:10.1002/joc.205
- Boyer TP, Antonov JJ, Baranova OK, Garcia H, Johnson DR, Locarnini RA, Mishonov AV, Pitcher MT, Smolyar I (2006) World Ocean Database 2009, vol 1. In: Levitus S (eds) Introduction, NOAA Atlas NESDIS, vol 66. NOAA, Silver Spring, Md, 219 pp
- Breivik Ø, Mogensen K, Bidlot J-R, Balmaseda MA, Janssen PAEM (2015) Surface wave effects in the NEMO ocean model: forced and coupled experiments. *J Geophys Res Oceans* 120:2973–2992. doi:10.1002/2014JC010565
- Carton JA, Giese BS (2008) A Reanalysis of Ocean Climate Using Simple Ocean Data Assimilation (SODA). *Mon Wea Rev* 136:2999–3017. doi:10.1175/2007MWR1978.1
- Cheng L et al (2017) Improved estimates of ocean heat content from 1960 to 2015. *Sci Adv* 3(3):e1601545. doi:10.1126/sciadv.1601545
- Cheng L, Zhu J, Abraham J (2015) Global upper ocean heat content estimation: recent progress and the remaining challenges. *Atmos Ocean Sci Lett* 8(6):333–338. doi:10.3878/AOSL20150031
- Compo GP, Whitaker JS, Sardeshmukh PD, Matsui N, Allan RJ, Yin X, Gleason BE, Vose RS, Rutledge G, Bessemoulin P, Brönnimann S, Brunet M, Crouthamel RI, Grant AN, Groisman PY, Jones PD, Kruk MC, Kruger AC, Marshall GJ, Maugeri M, Mok HY, Nordli Ø, Ross TF, Trigo RM, Wang XL, Woodruff SD, Worley SJ (2011) The twentieth century reanalysis project. *QJR Meteorol Soc* 137:1–28
- Daget N, Weaver AT, Balmaseda MA (2009) Ensemble estimation of background-error variances in a three-dimensional variational data assimilation system for the global ocean. *Q J R Meteorol Soc* 135:1071–1094
- Danabasoglu G, Yeager SG, Bailey D, Behrens E, Bentsen M, Bi D, Biastoch A, Böning C, Bozec A, Canuto VM, Cassou C (2014). North Atlantic simulations in coordinated ocean-ice reference experiments phase II (CORE-II). Part I: mean states. *Ocean Model* 73:76–107
- de Boissésou E, Balmaseda MA (2016) An ensemble of 20th century ocean reanalyses for providing ocean initial conditions for CERA-20C coupled streams. ECMWF ERA report Series issue 24. <http://www.ecmwf.int>. Accessed Aug 2017
- Dee DP, Uppala SM, Simmons AJ, Berrisford P, Poli P, Kobayashi S, Andrae U, Balmaseda MA, Balsamo G, Bauer P, Bechtold P (2011) The ERA-Interim reanalysis: configuration and performance of the data assimilation system. *Q J R Meteorol Soc* 137(656):553–597
- Dee DP, Balmaseda MA, Balsamo G, Engelen R, Simmons AJ, Thépaut JN (2014). Toward a consistent reanalysis of the climate system. *Bull Am Meteorol Soc* 95(8):1235–1248
- Durack PJ et al (2014) Quantifying underestimates of long-term upper-ocean warming. *Nat Clim Change* 4(11):999–1005. doi:10.1038/nclimate2389
- Enfield DB, Mestas-Nunez AM, Trimble PJ (2001) The atlantic multi-decadal oscillation and its relationship to rainfall and river flows in the continental US. *Geophys Res Lett* 28:2077–2080
- Giese BS, Seidel HF, Compo GP, Sardeshmukh PD (2016) An ensemble of ocean reanalyses for 1815–2013 with sparse observational input. *J Geophys Res Oceans* 121:6891–6910. doi:10.1002/2016JC012079
- Gille ST (2002) Warming of the Southern Ocean since the 1950s. *Science* 295:1275–1277
- Good SA, Martin MJ, Rayner NA (2013) EN4: quality controlled ocean temperature and salinity profiles and monthly objective analyses with uncertainty estimates. *J Geophys Res Oceans* 118:6704–6716. doi:10.1002/2013JC009067
- Gregory JM, Banks HT, Stott PA, Lowe JA, Palmer MD (2004) Simulated and observed decadal variability in ocean heat content. *Geophys Res Lett* 31:L15312. doi:10.1029/2004GL020258
- Griffies SM, Biastoch A, Böning C, Bryan F, Danabasoglu G, Chassignet EP, England MH, Gerdes R, Haak H, Hallberg RW, Hazelger W (2009) Coordinated ocean-ice reference experiments (COREs). *Ocean model* 26(1):1–46
- Griffies SM, Danabasoglu G, Durack PJ, Adcroft AJ, Balaji V, Böning CW, Chassignet EP, Curchitser E, Deshayes J, Drange H, Fox-Kemper B, Gleckler PJ, Gregory JM, Haak H, Hallberg RW, Heimbach P, Hewitt HT, Holland DM, Ilyina T, Jungclaus JH, Komuro Y, Krasting JP, Large WG, Marsland SJ, Masina S, McDougall TJ, Nurser AJG, Orr JC, Pirani A, Qiao F, Stouffer RJ, Taylor KE, Treguer AM, Tsujino H, Uotila P, Valdivieso M, Wang Q, Winton M, Yeager SG (2016). OMIP contribution to CMIP6: experimental and diagnostic protocol for the physical

- component of the Ocean Model Intercomparison Project. *Geosci Model Dev* 9:3231–3296. doi:10.5194/gmd-9-3231-2016
- Griffies SM, Yin J, Durack PJ, Goddard P, Bates SC, Behrens E, Bentsen M, Bi D, Biastoch A, Böning CW, Bozec A (2014) An assessment of global and regional sea level for years 1993–2007 in a suite of interannual CORE-II simulations. *Ocean Model* 78:35–89. doi:10.1016/j.ocemod.2014.03.004
- Gouretski V, Reseghetti F (2010) On depth and temperature biases in bathythermograph data: development of a new correction scheme based on analysis of a global ocean database. *Deep sea res Part I: oceanogr res pap* 57(6):812–833. doi:10.1016/j.dsr.2010.03.011
- He YC, Drange H, Gao Y, Bentsen M (2016) Simulated Atlantic meridional overturning circulation in the 20th century with an ocean model forced by reanalysis-based atmospheric data sets. *Ocean Model* 100:31–48
- Hersbach H, Peubey C, Simmons A, Berrisford P, Poli P, Dee D (2015) ERA-20CM: a twentieth-century atmospheric model ensemble. *QJR Meteorol Soc* 141:2350–2375. doi:10.1002/qj.2528
- Hirahara S, Balmaseda M, de Boissésion E, Hersbach H (2016) Sea Surface Temperature and Sea Ice Concentration for ERA5. ECMWF ERA Report Series issue 26
- Huang B, Zhu J, Marx L, Wu X, Kumar A, Hu ZZ, Balmaseda MA, Zhang S, Lu J, Schneider EK, Kinter III JL (2015) Climate drift of AMOC, North Atlantic salinity and arctic sea ice in CFSv2 decadal predictions. *Clim Dyn* 44(1–2):559–583
- Ingleby B (2010) Factors affecting ship and buoy data quality: a data assimilation perspective. *J Atmos Ocean Technol* 27(9):1476–1489
- Kent EC, Woodruff SD, Berry DI (2007). Metadata from WMO publication no. 47 and an assessment of voluntary observing ship observation heights in ICOADS. *J Atmos Ocean Technol* 24(2):214–234
- Laloyaux P, Balmaseda M, Dee D, Mogensen K, Janssen P (2016) A coupled data assimilation system for climate reanalysis. *QJR Meteorol Soc* 142:65–78. doi:10.1002/qj.2629
- Laloyaux P, de Boissésion E, Dalhgren P (2017) CERA-20C: an Earth system approach to reanalysis. ECMWF Winter Newsletter issue 150
- Large W, Yeager S (2004) Diurnal to decadal global forcing for ocean and seaice models: the data sets and climatologies. Technical Report TN-460+STR, NCAR, 105 pp. [https://www.researchgate.net/profile/Stephen\\_Yeager/publication/281588002\\_Diurnal\\_to\\_Decadal\\_Global\\_Forcing\\_for\\_Ocean\\_and\\_Sea\\_Ice\\_Models\\_The\\_Data\\_Sets\\_and\\_Flux\\_Climatologies/links/55eede7108ae199d47bfaf41.pdf](https://www.researchgate.net/profile/Stephen_Yeager/publication/281588002_Diurnal_to_Decadal_Global_Forcing_for_Ocean_and_Sea_Ice_Models_The_Data_Sets_and_Flux_Climatologies/links/55eede7108ae199d47bfaf41.pdf). Accessed Aug 2017
- Levitus S et al (2012) World ocean heat content and thermocline sea level change (0–2000 m), 1955–2010. *Geophys Res Lett* 39:L10603. doi:10.1029/2012GL051106
- Locarnini RA, Mishonov AV, Antonov JJ, Boyer TP, Garcia HE, Baranova OK, Zweng MM, Paver CR, Reagan JR, Johnson DR, Hamilton M, Seidov D (2013) World Ocean Atlas 2013, volume 1: temperature. In: Levitus S, Mishonov A (eds) NOAA Atlas NESDIS 73, p 40
- Madec G (2008) NEMO ocean engine, Tech. Rep.27, Notes du pôle de Modélisation—Institut Pierre-Simon Laplace, p 300
- Mantua NJ, Hare SR (2002) The Pacific decadal oscillation. *J Oceanogr* 58(1):35–44
- Mogensen K, Alonso Balmaseda M, Weaver A (2012) The NEMO-VAR ocean data assimilation system as implemented in the ECMWF ocean analysis for System 4. ECMWF Technical Memoranda No 668, February 2012. <http://www.ecmwf.int>. Accessed Aug 2017
- Müller WA, Matei D, Bersch M, Jungclaus JH, Haak H, Lohmann K, Compo GP, Sardeshmukh PD, Marotzke J (2015) A twentieth-century reanalysis forced ocean model to reconstruct the North Atlantic climate variation during the 1920s. *Clim Dyn* 44(7–8):1935–1955
- Palmer M, Balmaseda M, Chang Y-S, Chepurin G, Fujii Y, Good S, Guinehut S, Hernandez F, Martin, M, Masuda S, Peterson KA, Toyoda T, Valdivieso M, Vernieres G, Wang O, Xue Y (2014) CLIVAR-GSOP/GODAE Intercomparison of ocean heat content: initial results. *CLIVAR Exch* 19(1):8–10
- Palmer MD, Roberts CD, Balmaseda MA, Chang YS, Chepurin G, Ferry N, Fujii Y, Good SA, Guinehut S, Haines K, Hernandez F (2015) Ocean heat content variability and change in an ensemble of ocean reanalyses. *Clim Dyn*:1–22. doi:10.1007/s00382-015-2801-0
- Penduff T, Juza M, Barnier B, Zika J, Dewar WK, Treguier A-M, Molines JM, Audiffren N (2011) Sea-level expression of intrinsic and forced ocean variabilities at interannual time scales. *J Clim* 24:5652–5670. doi:10.1175/JCLI-D-11-00077.1
- Poli P, Hersbach H, Berrisford P, Dee DP, Simmons AJ, Laloyaux P (2013) The data assimilation system and initial performance evaluation of the ECMWF pilot reanalysis of the 20th-century assimilating surface observations only (ERA-20C). ERA Report Series
- Poli P, Hersbach H, Tan DGH, Dee DP, Thepaut JN, Simmons AJ, Peubey C, Laloyaux P, Komori T, Berrisford P, Dragani R, Trémolet Y, Hólm EV, Bonavita M, Isaksen L, Fisher M (2015) ERA-20C Deterministic, ERA report series No. 20
- Poli P, Hersbach H, Dee DP, Berrisford P, Simmons AJ, Vitart F, Laloyaux P, Tan DG, Peubey C, Thepaut JN, Trémolet Y (2016) ERA-20C: an atmospheric reanalysis of the twentieth century. *J Clim* 29(11):4083–4097
- Rhein M, Rintoul SR, Aoki S, Campos E, Chambers D, Feely RA, Gulev S, Johnson GC, Josey SA, Kostianoy A, Mauritzen C, Roemmich D, Talley LD, Wang F (2013) Observations: ocean. In: Stocker TF, Qin D, Plattner G-K, Tignor M, Allen SK, Boschung J, Nauels A, Xia Y, Bex V, Midgley PM (eds) climate change 2013: the physical science basis. Contribution of working group I to the fifth assessment report of the intergovernmental panel on climate change. Cambridge University Press, Cambridge
- Ricci S, Weaver AT, Vialard J, Rogel P (2005). Incorporating temperature-salinity constraints in the background error covariance of variational ocean data assimilation. *Mon Weather Rev* 133:317–338
- Stepanov VN, Haines K (2014) Mechanisms of Atlantic meridional overturning circulation variability simulated by the NEMO model. *Ocean Sci* 10(4):645–656
- Talandier C, Deshayes J, Treguier AM, Capet X, Benschila R, Debreu L, Dussin R, Molines JM, Madec G (2014) Improvements of simulated Western North Atlantic current system and impacts on the AMOC. *Ocean Model* 76:1–9
- Thomas BR, Kent EC, Swail VR, Berry DI (2008). Trends in ship wind speeds adjusted for observation method and height. *Int J Climatol* 28(6):747–763
- Titchner HA, Rayner NA (2014) The Met Office Hadley Centre sea ice and sea surface temperature data set, version 2: 1. Sea ice concentrations. *J Geophys Res Atmos* 119(6):2864–2889
- Tokinaga H, Xie S-P (2011) Wave- and anemometer-based sea surface wind (WASWind) for climate change analysis. *J Clim* 24(1):267–285. doi:10.1175/2010JCLI3789.1
- Trenberth KE, Marquis M, Zebiak S (2016) The vital need for a climate information system. *Nat Clim Change* 6(12):1057–1059
- Valdivieso M, Haines K, Balmaseda M, Chang YS, Drevillon M, Ferry N, Fujii Y, Köhl A, Storto A, Toyoda T, Wang X (2015) An assessment of air–sea heat fluxes from ocean and coupled reanalyses. *Clim Dyn*:1–26. doi:10.1007/s00382-015-2843-3
- Vancoppenolle M, Fichefet T, Goosse H, Bouillon S, Madec G, Maqueda MAM (2009) Simulating the mass balance and salinity

- of Arctic and Antarctic sea ice.1. Model description and validation. *Ocean Model* 27(1):33–53
- Vialard J, Weaver AT, Anderson DLT, Delecluse P (2003) Three- and four-dimensional variational assimilation with an ocean general circulation model of the tropical Pacific Ocean. Part 2: physical validation. *Mon Weather Rev* 131:1379–1395
- Weaver AT, Vialard J, Anderson DLT (2003) Three- and four-dimensional variational assimilation with a general circulation model of the tropical Pacific Ocean. Part I: formulation, internal diagnostics, and consistency checks. *Mon Weather Rev* 131:1360–1378
- Weaver AT, Deltel C, Machu E, Ricci S, Daget N (2005) A multivariate balance operator for variational ocean data assimilation. *Q J R Meteorol Soc* 131:3605–3625
- Willis JK, Roemmich D, Cornuelle B (2004) Interannual variability in upper ocean heat content, temperature, and thermocline expansion on global scales. *J Geophys Res* 109:C12036. doi:[10.1029/2003JC002260](https://doi.org/10.1029/2003JC002260)
- Yang C, Masina S, Storto A (2016) Historical ocean reanalyses (1900–2010) using different data assimilation strategies. *QJR Meteorol Soc*. doi:[10.1002/qj.2936](https://doi.org/10.1002/qj.2936)
- Zuo H, Balmaseda M, Mogensen K (2015) The ECMWF-MyOcean2 eddy-permitting ocean and sea-ice reanalysis ORAP5. Part 1: implementation. ECMWF Technical Memoranda No 736, February 2015. <http://www.ecmwf.int>. Accessed Aug 2017